Is Intercepted Current in an Ionic-Liquid Electrospray Thruster Actually Intercepted?

IEPC-2025-43

Presented at the 39th International Electric Propulsion Conference
Imperial College London, London, United Kingdom
14–19 September 2025

Oliver Jia-Richards[1]
University of Michigan, Ann Arbor, Michigan, USA

The standard interpretation of intercepted current in electrospray thrusters is direct impingement of the plume on any downstream electrodes as the plume leaves the thruster. In this paper we propose and analyze partial beam stalling as an alternative source of intercepted current in ionic-liquid electrospray thrusters. We show in simulation that low-energy ions created by the dissociation of heavy ion clusters are reflected by a potential barrier downstream of the thruster created due to the lack of explicit plume neutralization. These reflected ions impact the downstream surface of the extractor grid and are recorded as intercepted current, but may not contribute to key life-limiting mechanisms such as emitter-extractor propellant bridging. Simulation predictions of the intercepted current under this mechanism are consistent with trends in prior laboratory testing, which suggests that partial beam stalling may explain the vast majority of measured intercepted current for ionic-liquid electrospray thrusters.

I. Introduction

Intercepted current for electrospray thrusters refers to current measured on the extractor grid or any other electrode (e.g., an accelerator grid) downstream of the emitter. Understanding intercepted current is crucial for the design and operation of electrospray thrusters. Intercepted current is a form of transmission efficiency loss in electrospray thrusters as it represents charged particles that have been accelerated, but do not successfully leave the thruster to produce thrust. Along with reducing thrust, imbalances in intercepted current between a pair of bipolar electrospray thrusters can create challenges for spacecraft charging mitigation in paired neutralization architectures [1, 2]. Finally, accumulation of propellant on the thruster extractor grid due to interception can also influence the long-term performance of the thruster as well as limit its lifetime; in-space operation of liquid-metal electrospray thrusters has demonstrated that accumulation of conductive propellant changes the electrical configuration of the thruster [3], and propellant accumulation is hypothesized to be one of the primary lifetime limitations for electrospray thrusters as it can eventually lead to electrical shorting of the thruster, rendering it inoperable [4, 5].

Figure 1 shows a diagram of the standard interpretation of intercepted current; the beam generated by an individual electrospray emitter directly impinges on the downstream extractor grid as it leaves the thruster. This direct source of intercepted current is a straightforward explanation, and likely the cause of some intercepted current, particularly in multi-grid architectures such as those considered in Ref. [6]. Evidence for this source of intercepted current can be seen visually in Refs. [3] and [7], where accumulation of propellant

[1]Assistant Professor, Department of Aerospace Engineering, oliverjr@umich.edu

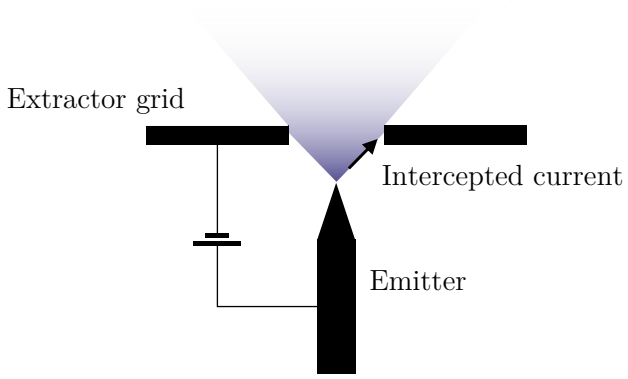


Fig. 1 Standard interpretation of measured intercepted current. The beam generated by an individual electrospray emitter impinges on the downstream extractor grid as it leaves the thruster.

on the extractor grid leads to shrinkage of the extractor aperture and the creation of propellant bridges between the extractor grid and emitter tip. Due to this inherent connection between intercepted current and propellant accumulation on the extractor grid, estimates of the intercepted current have been used as a way of monitoring propellant accumulation on the extractor grid, and reductions in intercepted current have been used as a proxy for improvements in overall thruster lifetime in lieu of performing extensive lifetime testing [5].

While it is clear that intercepted current due to direct impingement in the form suggested by Figure 1 likely occurs at the individual emitter level, it is worth considering if there may be alternative sources of intercepted current in electrospray thrusters. A primary driver of this consideration is that it is challenging to reconcile the direct impingement explanation of intercepted current with full-thruster measurements of intercepted current for passively-fed, single-grid electrospray thrusters formed by high-density planar arrays (e.g., those first developed in Refs. [8] and [9]). Characterization of an individual emitter for these arrays shows half-angle beam widths, in terms of current, of only ~5–10° with variations in the beam central axis (i.e., off-axis emission) of ~10° [10]. The design of passively-fed electrospray thrusters typically places the emitter tips flush with the base of a thin (<100 μm) extractor grid with wide aperture diameters of ~300–500 μm [7, 11] providing a nearly-hemispherical field of view for the emitter, yet tests of planar arrays still measure approximately 5% of the beam current as intercepted [7].

It is almost certain that direct interception in the form suggested by Figure 1 is occurring in full electrospray thruster arrays, particularly for a single erratic emitter, but it seems improbable that it can explain all of the intercepted current observed during full thruster testing unless a significant portion of the emitters on the array are behaving erratically. Our goal in this work is to understand if there are other sources of intercepted current beyond direct interception that can explain the intercepted current measured on full thruster arrays. If there are, then direct interception would not be responsible for all of the measured intercepted current, and it may not be possible to use intercepted current measured across an entire electrospray array as a proxy for thruster lifetime. Alternative sources of intercepted current may break the assumed correlation between intercepted current and propellant accumulation between the emitter tip and extractor grid, in particular by causing intercepted current to occur away from the emitter apertures.

In this paper we propose and analyze an alternative source of intercepted current specifically for ionic-liquid electrospray thrusters formed by high-density planar arrays. The essential idea is that the plume of ionic-liquid electrospray thrusters is typically not neutralized, particularly during laboratory testing. The un-neutralized plume creates a potential barrier downstream of the thruster, which can stall low-energy ions created by heavy ion cluster dissociation (e.g., low-energy monomers created by the dissociation of a heptamer). These low-energy ions are reflected back to the thruster, impinge on the downstream face of the extractor grid, and are recorded as intercepted current. Our hypothesis is that this partial beam stalling is responsible for some

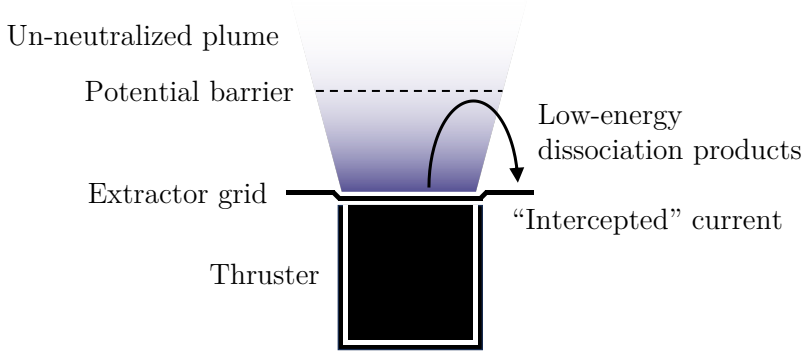


Fig. 2 Proposed interpretation of measured intercepted current based on the beam stalling hypothesis. The un-neutralized plume of an ionic-liquid electrospray thruster creates a potential barrier immediately downstream of the thruster. Low-energy ions created by ion cluster dissociation are reflected by the potential barrier, returning to the extractor grid, and are measured as intercepted current.

of the intercepted current measured in laboratory testing of ionic-liquid electrospray thrusters. Simulation predictions of the intercepted current under this mechanism are consistent with experimental measurements, supporting our hypothesis and indicating that partial beam stalling may be responsible for the majority of the intercepted current measured in laboratory testing of ionic-liquid electrospray thrusters.

II. Beam Stalling Hypothesis

The central hypothesis of this work is that some of the intercepted current measured during testing of ionic-liquid electrospray thrusters is caused by partial beam stalling. Figure 2 shows a diagram of this proposed mechanism, which is caused by the combination of two effects: the lack of plume neutralization and the creation of low-energy ions from ion cluster dissociation. The idea is that the lack of plume neutralization creates a potential barrier downstream of the thruster that stalls the low-energy dissociation products, and reflects them back to the downstream surface of the extractor grid. Since the entire surface of the extractor grid is typically conductive, these reflected ions are measured as intercepted current, despite not being directly intercepted as suggested in the standard interpretation of intercepted current shown in Figure 1. This section serves to provide initial theoretical justification for why we would expect to see beam stalling during testing of ionic-liquid electrospray thrusters ahead of the simulation study described in Sections III and IV.

Ionic-liquid electrospray thrusters are typically tested in a monopolar configuration without any explicit form of plume neutralization (e.g., a neutralizing cathode). During the operation of a full thruster array, the plumes of the individual emitters on the array combine and create a buildup of space charge immediately downstream of the thruster exhaust plane. This space charge in turn creates a potential barrier downstream of the thruster that serves to decelerate emitted ions [12]. Evidence for this space charge buildup can be seen in prior simulation studies of electrospray thruster arrays, which predicted the creation of potential barriers on the order of ~200 V, 10–20% of the typical acceleration potential of an ionic-liquid electrospray thruster, approximately 1–2 thruster diameters downstream of the thruster exhaust plane [13].

A potential barrier with magnitude of ~10–20% of the thruster acceleration potential would not cause beam stalling if all of the emitted ions have specific energies (i.e., energy per unit charge) equal to the thruster acceleration potential. In order for ions to be reflected by the potential barrier, which is required for beam stalling to occur, there needs to be a population of emitted ions that have specific energy $\lesssim$10–20% of the thruster acceleration potential. For ionic-liquid electrospray thrusters these low-energy ions can be created by the dissociation of ion clusters. Ionic liquids are composed of molecular cations, C^+, and anions, A^-, and the

charged particles emitted by an ionic-liquid electrospray thruster, assuming singly-charged particles, take the form of $(C^+A^-)_nC^+$ for a thruster operating in the positive polarity and $(C^+A^-)_nA^-$ for a thruster operating in the negative polarity, where n is the cluster's degree of solvation.

Most of the particles emitted by an ionic-liquid ion source, electrospray thrusters included, take the form of monomers, $n = 0$, and small ion clusters in the form of dimers, $n = 1$, and trimers, $n = 2$ [14]. However, there is experimental evidence of heavier ion clusters from tetramers to heptamers, $n = 3$–6, which compose a small (~2%) portion of the beam composition by current [15]. All ion clusters (i.e., not monomers) are known to be metastable and spontaneously dissociate during acceleration inside the thruster or almost immediately after leaving the thruster, producing neutral particles and a charged particle with a lower degree of solvation [16, 17]. The charged dissociation product carries the same speed and charge as the initial ion cluster but with a lower mass, causing a reduction in kinetic energy of the charged particle that is equal to the mass ratio of the initial ion cluster and the charged dissociation product. The charged dissociation product will continue to dissociate until the initial ion cluster has completely dissociated and the only remaining charged particle is a low-energy monomer traveling at the speed of the initial ion cluster.

For an ionic liquid with cations and anions of similar mass, the ratio of the kinetic energy of the low-energy monomer at the end of the dissociation chain relative to that of the initial ion cluster is

$$\frac{KE_\mathrm{m}}{KE_\mathrm{i}} = \frac{1}{2n_\mathrm{i} + 1} \tag{1}$$

where subscripts m and i correspond to the resulting low-energy monomer and initial ion cluster respectively, and it is assumed that there is minimal change in the background potential during the dissociations. If the initial ion cluster is a heptamer, $n = 6$, which is known to exist in the emitted beams of ionic liquid ion sources [15], then the resulting kinetic energy ratio is 0.077. Assuming the potential energy of the charged particle is negligible at dissociation, then the specific energy of a monomer created due to complete dissociation of a heptamer is only ~7.7% of the thruster acceleration potential. This low-energy monomer would certainly be reflected by the 10–20% potential barrier predicted from prior simulations [13], and could return to the thruster extractor grid assuming minimal motion radially away from the thruster's central axis.

This initial analysis provides theoretical justification for our beam stalling hypothesis. We have experimental evidence of sufficiently heavy metastable ion clusters that will dissociate down to low-energy ions with specific energies only a small fraction (~5–10%) of the thruster acceleration potential [15], and simulation evidence of a downstream potential barrier approximately 10–20% of a typical thruster acceleration potential [13]. These two aspects combined could create the conditions necessary for partial beam stalling in the plumes of ionic-liquid electrospray thrusters, and in turn provide an alternative source of intercepted current. Our goal throughout the rest of this paper is to demonstrate this mechanism by simulating the plume of an ionic-liquid electrospray thruster, and comparing the simulation predictions of the intercepted current to prior experimental data in order to provide further support for our hypothesis.

III. Approach

In order to properly test our beam stalling hypothesis, we simulated the exhaust plume of four different electrospray thrusters in configurations representative of prior experimental studies, tracked any intercepted current due to beam stalling for different emission currents, and then compared the simulation predictions to the experimental measurements. All simulations were conducted using the particle-in-cell method [18, 19] using an axisymmetric simulation domain, diagrammed in Figure 3. The axisymmetric domain reduces the spatial dimensions, and therefore computational complexity, of the simulation while still capturing the essential processes in the plume evolution (e.g., the formation of a downstream potential barrier).

The simulation domain used in this study is representative of laboratory testing of a monopolar electrospray thruster in a cylindrical vacuum chamber. The axial and radial extents of the simulation domain correspond to the length, $L_z = 50$ cm, and radius, $L_r = 20$ cm of the vacuum chamber. A closed simulation domain was

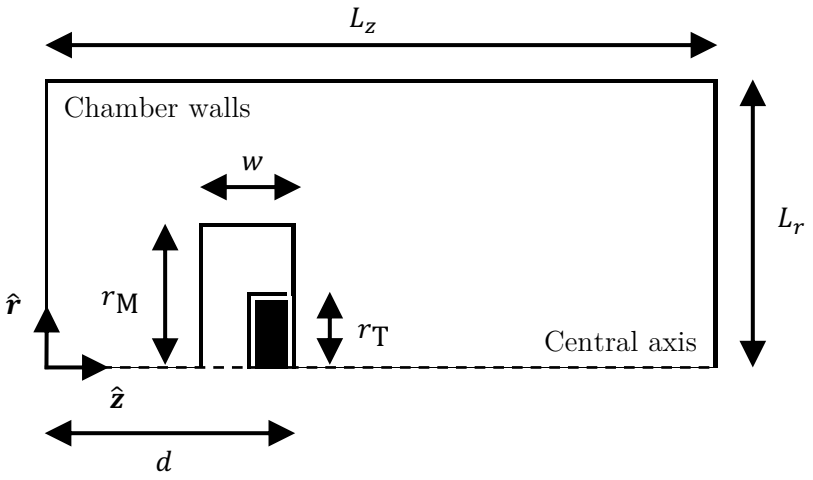


Fig. 3 Diagram of the axisymmetric simulation domain consisting of a cylindrical vacuum chamber of length L_z and radius L_r, a cylindrical thruster mount of radius r_{M} and width w, and a cylindrical thruster of radius r_{T}, all aligned by their central axes. The front of the mount and thruster extractor grid are aligned and a distance d from the back of the chamber. The chamber walls, mount, and thruster extractor grid are grounded, and the mount and thruster extractor grid are electrically connected.

selected in order emulate testing in a closed vacuum chamber and to avoid issues with artificial potential inflation that can occur with open simulation boundaries, which has been a concern in prior electrospray simulations [13, 20]. The walls of the vacuum chamber are assumed to be grounded.

An axisymmetric thruster of radius r_T is housed in a thruster mount of radius r_M and width $w = 2$ cm, and the front of the thruster extractor grid positioned a distance $d = 5$ cm from the back of the vacuum chamber. Both the thruster and mount radii vary with simulation test case. The downstream surface of the thruster mount is electrically connected to the thruster extractor grid such that any charged particles which impact the downstream surface of the thruster mount or the thruster extractor grid are recorded as intercepted current. This modeling choice emulates the fact that for many electrospray thrusters the size of the extractor grid is much larger than the size of the emitter array (e.g., see Ref. [11]). Similar to the vacuum chamber walls, the surfaces of the thruster mount and the thruster extractor grid are assumed to be grounded.

We model the thruster as a uniform emitting disk with emission directed in the $+\hat{z}$ direction, and do not model individual emitters nor account for any spatial non-uniformity of emission [21]. The acceleration potential and emission current density vary between simulation test cases. Particles are emitted from the thruster with a specific energy deficit of 5 V relative to the thruster acceleration potential and spread of 10 V, consistent with experimental data [16], and the angular distribution of emission current density relative to the $+\hat{z}$ direction corresponds to a cosine distribution

$$j(\theta) = 1 + \cos\left(\pi\theta/\theta_0\right); \quad \theta \in [0, \theta_0] \tag{2}$$

where $\theta_0 = 15^\circ$ is the maximum divergence angle of the emitted plume. This emission profile closely matches experimental current density profiles (e.g., that of Ref. [14]) while being simple to implement. All emitted particle species are assumed to be emitted from the thruster with the same angular distribution profile, and we do not model possible dependences of the angular distribution profile with emitted species [10].

Table 1 shows the plume species composition used for all simulation test cases. The plume predominantly consists of monomers, dimers, and trimers ($n = 0$–2) with 10% of the species composition, by current, evenly distributed between heavy ion clusters of tetramers up to heptamers ($n = 3$–6). The intent of this species

Table 1 Plume species composition and mean species lifetime used for all simulation testing.

Degree of solvation, n	0	1	2	3	4	5	6
Current fraction	0.4	0.3	0.2	0.025	0.025	0.025	0.025
Mean lifetime [μs]	N/A	1.5	0.15	0.01	0.01	0.01	0.01

composition is to represent a plausible species composition for the plume of an ionic-liquid electrospray thruster. The beam stalling hypothesis implies that time-of-flight mass spectrometry measurements for ionic-liquid electrospray thrusters would not be able to measure the presence of heavy ion clusters in the plume, since they would not reach the time-of-flight detector, which implies that the plume species composition from prior thruster testing is unknown. For this composition, the plume is dominated by monomers and light ion clusters while containing the heavy ion clusters necessary to observe potential beam stalling.

After emission from the thruster, the spontaneous dissociation of all ion clusters ($n \geq 1$) was modeled as a constant rate process defined by a mean lifetime [17]. Reliable experimental data for the lifetime of ion clusters is only available for dimers, but there is experimental evidence that suggests that the dissociation rate of heavier ion clusters, trimers and above, increases with degree of solvation [16, 17]. Table 1 also shows the mean lifetime for all metastable ion clusters used in this work. The mean lifetime of dimers was selected to closely match the measured mean lifetime of EMI-BF_4 dimers [17] while the mean lifetime of heavier ion clusters was arbitrarily selected in order to enforce fast dissociation. All dissociation events were modeled as single-step dissociations such that the degree of solvation only decreases by one during each dissociation.

In addition to ion cluster dissociation in the exhaust plume, we also modeled internal dissociation of ion clusters during acceleration inside the thruster [22]. The species composition in Table 1 sets the species composition of the plume immediately after emission (i.e., at the emitter tip). In this work we assumed that 50% of those ion clusters for each species dissociate inside the thruster before leaving the extractor grid. This internal dissociation was modeled as a single-step dissociation with dissociation rate that is constant with respect to the local potential. The result of this dissociation rate is that the specific energy of the emitted ions, and therefore ion exhaust speeds, is a continuum between the discrete values for each species under the assumption of no internal dissociation, which is experimentally visible as sloped transitions between the discrete steps of both time-of-flight and retarding-potential-analysis data [17, 22].

For the particle-in-cell setup, the domain was discretized into a uniform mesh with 301 mesh points along each axis. At each simulation step, 300 macroparticles were injected into the simulation domain, uniformly distributed across the thruster and with a velocity distribution given by the specific energy and angular distributions defined above. The macroparticles were randomly assigned a species according to the species composition in Table 1, and the macroparticle weight was selected such that the overall emission current was equal to a user-defined value. Any internal dissociation of the ion cluster was considered prior to particle injection into the simulation domain. The simulation time step was adaptively selected in order to ensure that no particle travels more than half the grid spacing along each axis at each step, meeting the requirements of the Courant-Friedrichs-Lewy condition. Finally, particles that impact the walls of the vacuum chamber, surface of the thruster mount, or extractor grid were assumed to be neutralized with no secondary species emission, effectively removing them from the simulation as only charged particles were tracked.

The parameters that were varied between each simulation test case were the thruster and mount radii, in order to model different thruster configurations, as well as the thruster acceleration potential and emission current, in order to model different operating conditions. Unless otherwise specified, all other parameters are fixed at their values listed above for all simulation test cases. Each simulation was first run for 30 μs in order to allow the plume to reach its steady-state configuration in the vacuum chamber. Then the intercepted current on the extractor grid and downstream surface of the thruster mount was monitored for a further 10 μs (40 μs total simulation time), averaged over that time span, and returned as the primary simulation output.

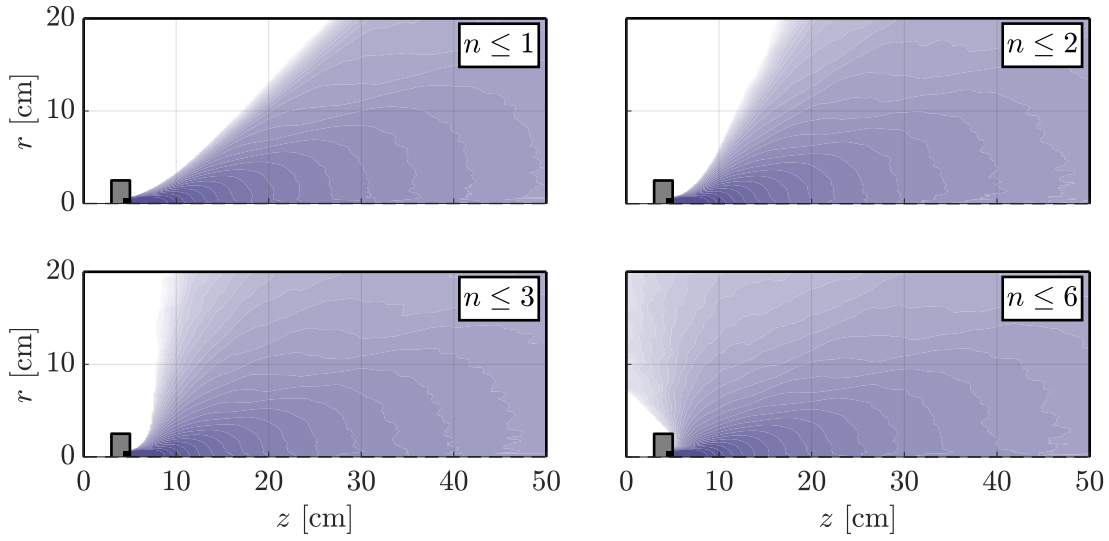


Fig. 4 Qualitative comparison of the charge density downstream of an ionic-liquid electrospray thruster for different maximum ion cluster degrees of solvation. Contour levels are shown on a logarithmic scale with consistent color mapping between plots. Note that return current due to beam stalling is only present when heavy ion clusters (e.g., heptamers, $n = 6$) are included in the simulation.

IV. Results

As a first simulation we result, we can test our initial justification for the beam stalling hypothesis, outlined in Section II. Figure 4 shows a qualitative comparison of the steady-state charge density downstream of an ionic-liquid electrospray thruster of radius 0.56 cm, which gives a total emission area of 1 cm^2, operating at an acceleration potential of 1 kV and emission current of 100 μA, with a thruster mount radius of 2.5 cm. Each plot shows the how the downstream charge density profile changes for different maximum emitted degrees of solvation. The top-left plot shows a plume with a maximum degree of solvation of $n = 1$, which is the typical maximum degree of solvation considered in many electrospray simulations [20, 23]. The plume is only composed of monomers and dimers, in a 1-1 ratio, and is consistent with prior electrospray simulation results [13, 20]; within a few thruster radii the plume rapidly diverges from its angular distribution at emission out to plume half angles of ~45°, consistent with experimental measurements of the current density distribution downstream of an ionic-liquid electrospray thruster (e.g., Ref. [7]).

The top-right and bottom-left plots in Figure 4 show the impact of including trimers and tetramers respectively in the simulation. The plume in the top-right plot contains ions with degrees of solvation of $n \in \{0, 1, 2\}$ in a 2-2-1 ratio and the plume in the bottom-left plot contains ions with degrees of solvation of $n \in \{0, 1, 2, 3\}$ in a 4-3-2-1 ratio. The key point is that as the maximum degree of solvation in the emitted plume increases, the divergence of the plume increases as expected. As we add heavier and heavier ion clusters to the simulation we produce monomer dissociation products with lower and lower energies, according to Eq. 1, which are more easily deflected by the downstream potential barrier. However, in neither of these cases would there be an intercepted current due to beam stalling. The low-energy dissociation products are significantly deflected away from the plume centerline, but are not reflected back to the thruster.

Once the maximum degree of solvation in the simulation increases to heptamers, $n = 6$, we start to see reflection of the low-energy dissociation products back to the thruster. The bottom-right plot of Figure 4 shows a plume with the beam composition given in Table 1. Clearly visible is a population of ions that have been reflected by the downstream potential barrier and have velocities in the negative axial direction (i.e.,

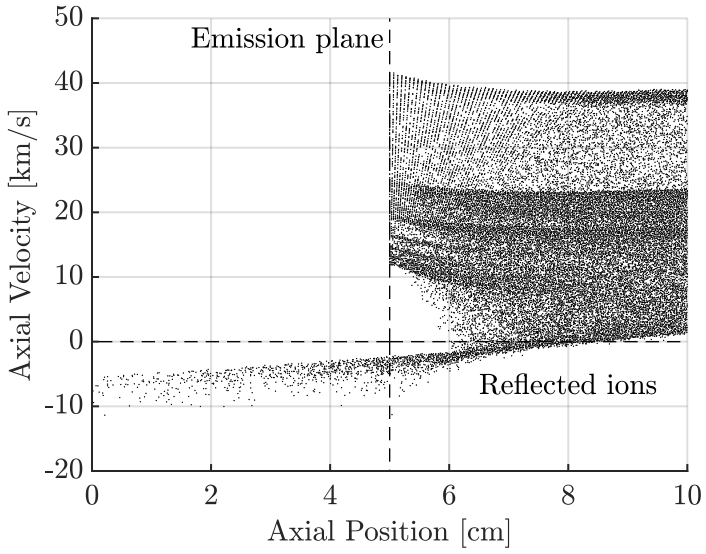


Fig. 5 Scatter plot of the axial positions and velocities of ions emitted from a representative ionic-liquid electrospray thruster with the plume composition of Table 1, with the thruster emission plane located at an axial position of 5 cm. The ions reflected by the downstream potential barrier are those with negative axial velocities, and generate a return current if they collide with the thruster.

opposite the intended emission direction). These reflected ions are the very-low-energy monomers created by complete dissociation of heavy ion clusters, primarily hexamers and heptamers. Many of these ions do not impact the thruster mount due to their radial velocity. However, a small population of these ions does impact the downstream face of the thruster mount and would be registered as intercepted current.

Figure 5 shows this effect in more detail through a scatter plot of the axial positions and velocities of the simulation macroparticles. Particles are injected into the simulation domain at an axial position of 5 cm, corresponding to dimension d in Figure 3, with velocities directed in the positive axial direction. The downstream potential barrier decelerates all of the ions as the plume propagates, but for monomers and the dissociation products of lighter ion clusters the deceleration is not sufficient to cause beam stalling. Only for the dissociation products of heavy ion clusters is the deceleration sufficient to cause beam stalling, visible by the population of ions with negative axial velocities. Most of these ions do not impact the thruster mount, visible from particles in Figure 5 with negative axial velocity but axial position less than $d = 5$ cm, but some do, and will be registered as intercepted current.

While these results so far indicate that an intercepted current due to partial beam stalling could be created, it is unclear how important the effect is for the testing of electrospray thrusters. To understand the importance of intercepted current from partial beam stalling, we can compare the simulation predictions to prior experimental studies. Table 2 provides a list of prior experimental studies that tested full ionic-liquid thrusters, and where the measured intercepted current at different thruster operating conditions, thruster acceleration voltage and emission current, are easily extractable from the published data. For comparison we ran our plume simulation at each operating condition with thruster and mount radii selected to match estimates of the emission and extractor grid areas (e.g., a 1 cm^2 thruster corresponds to a thruster radius of 0.56 cm).

The thruster and mount radii listed in Table 2 are based on educated guesses (e.g., a visual estimate from a picture of the thruster), and should not be construed as accurate information on the geometry of the thruster from the study. In particular, the vast majority of ionic-liquid electrospray thrusters use rectangular emitter arrays and mounts whereas our axisymmetric simulation requires conversion to equivalent circular

Table 2 Thruster and mount radii used in the simulation to match estimates of the emission and extractor grid areas for each experimental study. These values are estimates generated for the purpose of this study, and should not be construed as accurate geometric information.

Experimental study	Thruster radius, r_T [cm]	Mount radius, r_M [cm]
Natisin et al., 2021 [11]	0.73	2.14
Ma et al., 2021 [24]	1.13	2.26
Corrado et al., 2024 [25]	0.37	0.74
Whittaker et al., 2025 [26]	4.45	5.02

geometries. Due to this geometric discrepancy as well as our lack of information on the plume composition at emission, we do not anticipate being able to accurately predict the exact intercepted current due to beam stalling for each study. Instead, our goal is to compare trends in the predicted and measured intercepted current across operating conditions. If the trends are similar (i.e., the simulation predictions and experimental measurements differ by a constant scalar factor) then our assumption is that the differences in absolute value of the intercepted current are caused by geometric discrepancies or the unknown plume composition.

Figure 6 shows the resulting comparison of simulation prediction and experimentally measured intercepted current versus emission current for all four studies, each shown on a different plot, listed in Table 2. The three lines show the experimental data extracted from the corresponding publication, the raw prediction of our simulation using the estimated geometric parameters and beam composition given in Tables 1 and 2, and a scaled simulation result. The scaled simulation data was generated by multiplying the simulated intercepted current by a constant scaling factor in order to account for potential geometric discrepancies and the unknown plume composition. The scaling factor is unique to each study, and was calculated by minimizing the root mean square error of the raw simulation data multiplied by the scaling factor relative to the experimental data.

The key result is that for three of the four studies, the scaled simulation data closely tracks the measured experimental data. These three studies represent three different thrusters that were designed for different sizes, utilized both internally- (i.e., porous) and externally-wetted emitters, characterized by three different research groups in different experimental facilities, and operated at three different emission current ranges. Yet in all three cases the experimentally-measured trend in intercepted current as a function of emission current can be almost entirely explained by partial beam stalling as an alternative to direct interception.

For the study where the experimental and scaled simulation data do not align (Ma et al., 2021 [24]), it is notable that the average emitter current, ~100 μA/emitter, is higher than the typical average emitter current of the other studies, $\lesssim$1 μA/emitter. The emitters are of a similar design to those in the other studies, but are operating at a highly-stressed operating point, potentially increasing the probability of erratically-behaving emitters and direct intercepted current (i.e., that of Figure 1). Evidence for this is that the intercepted current fraction is relatively high, ~37% compared to the 2–5% of the other studies, and increases linearly with emission current, which would be expected if the plumes of the emitters were directly impinging on the extractor grid; if the emitted current doubles then twice as much current impinges on the extractor grid, assuming minimal change in the plume shape. For the other three studies, where the experimental and scaled simulation data do align, the relationship is distinctly nonlinear, and specifically superlinear.

These result provide further support for the beam stalling hypothesis; our simulations are able to predict the trend in intercepted current as a function of emission current across a variety of thruster designs, as long as the thruster appears to be operating in regime where the emitters would not be highly stressed (i.e., average emission currents of $\lesssim$1 μA/emitter). In these cases, the intercepted current fraction remains low ($\lesssim$5%), and the trend in the intercepted current with increasing emission current is superlinear. This result does rely on the underlying assumption that the geometric discrepancies and unknown plume species composition can be accounted for with a constant scaling factor on the raw simulation data.

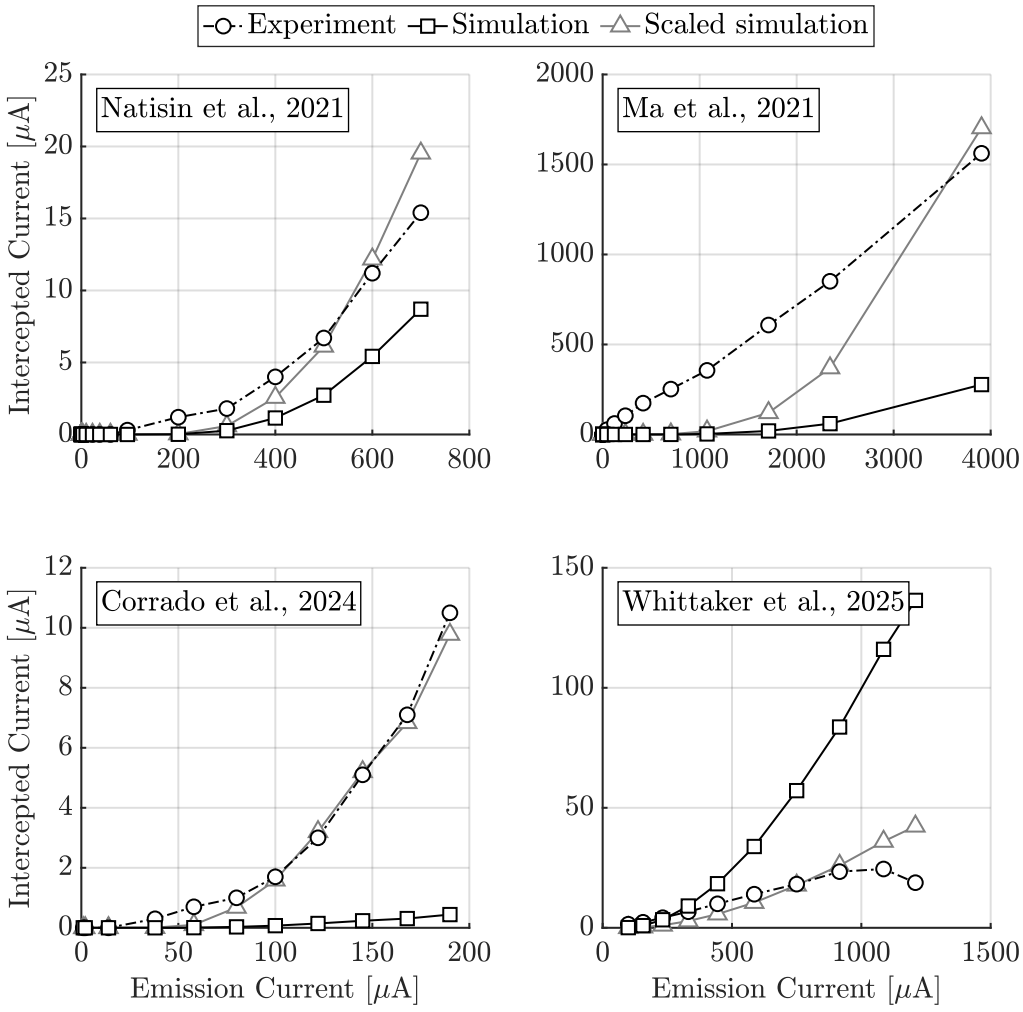


Fig. 6 Comparison of simulation predictions of the intercepted current for different ionic-liquid electrospray thruster experimental studies with the measured experimental data. The scaled simulation data was generated by multiplying the simulated intercepted current by a constant scaling factor, unique to each study, chosen to minimize the root mean square error relative to the experimental data.

V. Conclusion

This study demonstrates that intercepted current for ionic-liquid electrospray thrusters can be generated by partial beam stalling, where low-energy ions created by the dissociation of heavy ionic-liquid clusters are reflected by a downstream potential barrier back to the extractor grid. Our simulation results show that low-energy monomers from the complete dissociation of hexamers and heptamers, the heaviest ion clusters in our simulation, are stalled by the downstream potential barrier caused by the lack of any explicit plume neutralization. In addition, we were able to use partial beam stalling in order to accurately predict, within an constant scaling factor, the intercepted current for multiple prior experimental characterizations of ionic-liquid electrospray thrusters across a range of thruster designs, sizes, and experimental facilities.

The first key consequence of these results is that there is an alternative source of intercepted current in ionic-liquid electrospray thrusters beyond direct interception. For thrusters with well-aligned and not-overly-stressed emitters, our results suggest that partial beam stalling is actually responsible for the vast majority of measured intercepted current. This result breaks the commonly-assumed link between intercepted current and life-limiting mechanisms for electrospray thrusters; the charged particles forming the intercepted current as a result of partial beam stalling impinge on the downstream surface of the extractor grid, as opposed to internal surfaces, and may impact the extractor grid far away from the emitter apertures. These particles would not contribute towards the formation of an emitter-extractor propellant bridge, so differences in intercepted current between designs may not be a reliable way of predicting changes in overall thruster lifetime.

A second consequence is that indirect experimental characterization techniques for ionic-liquid electrospray thrusters, time-of-flight mass spectrometry and retarding-potential analysis, may not provide an accurate assessment of a thruster's performance characteristics. If the plume has partially stalled, then low-energy monomers generated by the dissociation of heavy ion clusters will not reach the instrument detector. These low-energy monomers carry the information associated with the presence of heavy ion clusters in the emitted plume, so if they do not reach the detector then the presence of the heavy ion clusters will not be measured. Our results may explain why the plumes of some ionic-liquid electrospray thrusters appear to be free of heavy ions [27, 28] and also have significant implications for anomalous mass loss [11]; the presence of heavy ion clusters in the plume will be hidden from time-of-flight measurements by beam stalling, causing any estimates of the thruster's mass flow rate from time-of-flight data to be an underestimate of the true mass flow rate.

A final, and heavily related, consequence is that testing of single emitters may be crucial for understanding the performance of ionic-liquid electrospray thrusters. Our simulations were based on assuming that emission characteristics (e.g., plume angular distributions) at the extractor grid exit plane for full ionic-liquid electrospray thrusters were similar to those of single-emitter ionic-liquid ion sources. Given that we were able to to predict measurement characteristics using this assumption, single-emitter studies may provide a reliable way of probing the plume characteristics at emission for full thrusters due to their much lower charge densities, therefore lessening the impact of space-charge effects. Thorough characterization of single emitters, such as with angularly-dependent time-of-flight studies [29], may provide more insight into the performance of ionic-liquid electrospray thrusters relative to directly testing the thruster itself. Connecting these single-emitter studies to full-thruster performance would be additionally aided by research into the effects of emitter multiplexing on the emission characteristics of individual emitters on a thruster array.

Further support for the results of this study could be obtained through additional, dedicated experiments with ionic-liquid electrospray thrusters. A simple experiment to confirm the results of this work could use collector plate that is concentric with the thruster and aligned with the extractor grid exit plane. Low-energy ions reflected by the downstream potential barrier would impinge on the collector plate and provide direct confirmation for the presence of partial beam stalling, if a current is measured. A series of concentric collector plates at different radii from the thruster centerline would provide spatial information on the reflected ions. When coupled with plume simulations, such as the one utilized in this work, the spatial information could be used to infer emission properties such as the angular distribution and plume species composition.

Acknowledgements

This research was supported in part through computational resources and services provided by Advanced Research Computing at the University of Michigan, Ann Arbor.

References

[1] Mier-Hicks, F., and Lozano, P. C., "Spacecraft-Charging Characteristics Induced by the Operation of Electrospray Thrusters," *Journal of Propulsion and Power*, Vol. 33, No. 2, 2017, pp. 456–467. https://doi.org/10.2514/1.B36292.

[2] Courtney, D. G., Shea, H., Dannenmayer, K., and Bulit, A., "Charge Neutralization and Direct Thrust Measurements from Bipolar Pairs of Ionic Electrospray Thrusters," *Journal of Spacecraft and Rockets*, Vol. 55, No. 1, 2018, pp. 54–65. https://doi.org/10.2514/1.A33863.

[3] Krejci, D., et al., "Extractor Electrode Clogging in FEEP Propulsion and In-Space Mitigation Demonstration," *Journal of Electric Propulsion*, Vol. 4, No. 26, 2025. https://doi.org/10.1007/s44205-025-00127-z.

[4] Anderson, G., et al., "Experimental results from the ST7 mission on LISA Pathfinder," *Physical Review D*, Vol. 98, No. 102005, 2018. https://doi.org/10.1103/PhysRevD.98.102005.

[5] Thuppul, A., Wright, P. L., Collins, A. L., Ziemer, J. K., and Wirz, R. E., "Lifetime Considerations for Electrospray Thrusters," *Aerospace*, Vol. 7, No. 108, 2020. https://doi.org/10.3390/aerospace7080108.

[6] Dandavino, S., et al., "Microfabricated Electrospray Emitter Arrays with Integrated Extractor and Accelerator Electrodes for the Propulsion of Small Spacecraft," *Journal of Micromechanics and Microengineering*, Vol. 24, No. 075011, 2014. https://doi.org/10.1088/0960-1317/24/7/075011.

[7] Krejci, D., Mier-Hicks, F., Thomas, R., Haag, T., and Lozano, P., "Emission Characteristics of Passively Fed Electrospray Microthrusters with Propellant Reservoirs," *Journal of Spacecraft and Rockets*, Vol. 54, No. 2, 2017, pp. 447–458. https://doi.org/10.2514/1.A33531.

[8] Velásquez-García, L. F., Akinwande, A. I., and Martínez-Sánchez, M., "A Planar Array of Micro-Fabricated Electrospray Emitters for Thruster Applications," *Journal of Microelectromechanical Systems*, Vol. 15, No. 5, 2006, pp. 1272–1280. https://doi.org/10.1109/jmems.2006.879710.

[9] Courtney, D., Li, H. Q., and Lozano, P., "Emission Measurements from Planar Arrays of Porous Ionic Liquid Ion Sources," *Journal of Physics D: Applied Physics*, Vol. 45, No. 485203, 2012. https://doi.org/10.1088/0022-3727/45/48/485203.

[10] Schroeder, M. R., Gallud, X., Bruno, A. R., Jia-Richards, O., and Lozano, P. C., "Angular Properties of Ionic Liquid Electrospray Emitters," *AIAA SciTech Forum*, American Institute of Aeronautics and Astronautics, National Harbor, MD, USA, 2023. https://doi.org/10.2514/6.2023-1408.

[11] Natisin, M. R., et al., "Efficiency Mechanisms in Porous-Media Electrospray Thrusters," *Journal of Propulsion and Power*, Vol. 37, No. 5, 2021, pp. 650–659. https://doi.org/10.2514/1.B38160.

[12] Deng, W., and Gomez, A., "Influence of Space Charge on the Scale-Up of Multiplexed Electrosprays," *Aerosol Science*, Vol. 38, No. 10, 2007, pp. 1062–1078. https://doi.org/10.1016/j.jaerosci.2007.08.005.

[13] Smith, A. G., and Petro, E. M., "Propagating an Electrospray Emission Model to Array Scales Using Particle-in-Cell," *Journal of Propulsion and Power*, Vol. 40, No. 5, 2024, pp. 677–690. https://doi.org/10.2514/1.B39400.

[14] Lozano, P., and Martínez-Sánchez, M., "Ionic Liquid Ion Sources: Characterization of Externally Wetted Emitters," *Journal of Colloid and Interface Science*, Vol. 282, No. 2, 2005, pp. 415–421. https://doi.org/10.1016/j.jcis.2004.08.132.

[15] Jia-Richards, O., "Quantification of Ionic-Liquid Ion Source Beam Composition from Time-of-Flight Data," *Journal of Applied Physics*, Vol. 132, No. 7, 2022, p. 074501. https://doi.org/10.1063/5.0094699.

[16] Lozano, P. C., "Energy Properties of an EMI-Im Ionic Liquid Ion Source," *Journal of Physics D: Applied Physics*, Vol. 39, No. 1, 2006, pp. 126–134. https://doi.org/10.1088/0022-3727/39/1/020.

[17] Miller, C. E., and Lozano, P. C., "Measurement of the Dissociation Rates of Ion Clusters in Ionic Liquid Ion Sources," *Applied Physics Letters*, Vol. 116, No. 254101, 2020. https://doi.org/10.1063/5.0006529.

[18] Tskhakaya, D., Matyash, K., Schneider, R., and Taccogna, F., "The Particle-in-Cell Method," *Contributions to Plasma Physics*, Vol. 47, No. 8-9, 2007, pp. 563–594. https://doi.org/10.1002/ctpp.200710072.

[19] Brieda, L., *Plasma Simulations by Example*, 1st ed., CRC Press, Boca Raton, FL, USA, 2019. https://doi.org/10.1201/9780429439780.

[20] Asher, J. S., and Wang, J., "Three-Dimensional Particle-in-Cell Simulations of Bipolar Ionic Electrospray Thruster Plume," *Journal of Propulsion and Power*, Vol. 38, No. 4, 2022, pp. 573–580. https://doi.org/10.2514/1.B38610.

[21] Guerra-Garcia, C., Krejci, D., and Lozano, P., "Spatial Uniformity of the Current Emitted by an Array of Passively Fed Electrospray Porous Emitters," *Journal of Physics D: Applied Physics*, Vol. 49, No. 115503, 2016. https://doi.org/10.1088/0022-3727/49/11/115503.

[22] Courtney, D. G., and Shea, H., "Fragmentation in Time-of-Flight Spectrometry-Based Calculations of Ionic Electrospray Thruster Performance," *Journal of Propulsion and Power*, Vol. 31, No. 5, 2015, pp. 1500–1504. https://doi.org/10.2514/1.B35837.

[23] Park, I., Moon, G., Takao, Y., and Jun, E., "Analysis of Oscillatory Local Neutralization According to Fragmentation in the Ionic Liquid Electrospray Thruster Plume," *Physics of Plasmas*, Vol. 32, No. 3, 2025, p. 033511. https://doi.org/10.1063/5.0249312.

[24] Ma, C., Bull, T., and Ryan, C., "Plume Composition Measurements of a High-Emission-Density Electrospray Thruster," *Journal of Propulsion and Power*, Vol. 37, No. 6, 2021, pp. 816–831. https://doi.org/10.2514/1.B37996.

[25] Corrado, M. N., et al., "Performance Characterization of High-Density Electrospray Thrusters," *International Electric Propulsion Conference*, Electric Rocket Propulsion Society, Toulouse, France, 2024.

[26] Whittaker, C., Arestie, S., Marrese-Reading, C., and Jorns, B., "Characterization of a 10 W Class Electrospray Array Thruster," *Journal of Electric Propulsion*, Vol. 4, No. 20, 2025. https://doi.org/10.1007/s44205-025-00114-4.

[27] Lyne, C. T., Liu, M. F., and Rovey, J. L., "Tandem Energy-Analyzer/Mass-Spectrometer Measurements of an Ionic Liquid Ion Source," *Journal of Propulsion and Power*, Vol. 40, No. 5, 2024, pp. 759–768. https://doi.org/10.2514/1.B39396.

[28] Naemura, M., and Takao, Y., "Direct Detection of Neutral Species from Ionic Liquid Electrospray Thrusters in the Purely Ionic Regime," *Review of Scientific Instruments*, Vol. 96, No. 7, 2025, p. 073302. https://doi.org/10.1063/5.0258187.

[29] Ulibarri, Z., and Petro, E., "Direct Two-Dimensional Goniometric Steering of Vacuum Electrospray Ion Beams for Angular Time-of-Flight Studies," *Review of Scientific Instruments*, Vol. 96, No. 4, 2025, p. 043301. https://doi.org/10.1063/5.0240136.